Fermi National Accelerator Laboratory

FERMILAB-Pub-86/145
0102.000
1111.000

Characteristics of Inelastic Interactions of High Energy Hadrons with Atomic Electrons *

S. Qian and A. Van Ginneken
Fermi National Accelerator Laboratory
P.O. Box 500
Batavia, IL 60510

October 1986

*Submitted to Nucl. Instrum. Methods A

CHARACTERISTICS OF INELASTIC INTERACTIONS OF HIGH ENERGY HADRONS WITH ATOMIC ELECTRONS

S. Qian and A. Van Ginneken

Fermi National Accelerator Laboratory
P.O. Box 500, Batavia, IL, 60510.

October, 1986

ABSTRACT

The energy loss and angular characteristics of the inelastic interactions of high energy protons and pions (up to 30 TeV) with atomic electrons are analyzed in the electron rest frame. Inclusive distributions of the incident hadron, recoiling electron and produced pions are obtained along with the rms angles of these particles as a function of their momentum. The results are suitably parametrized for use in Monte Carlo simulations. For the incident hadron the average energy loss and rms angle in bulk matter are determined and compared with other processes. The contribution to dE/dx from inelastic processes exceeds that of competing processes in the multi-TeV regime.

1. Introduction

The current interest in the design and exploitation of multi-TeV proton colliders provides an incentive to revise the computer codes needed to study particle transport in bulk matter. Such a revision is prompted by the onset, around 1 TeV, of rather dramatic changes in relative importance of the basic processes responsible for energy loss and angular diffusion of charged particles in bulk matter. In ref. 1 results of some calculations on this subject are presented for bremsstrahlung, pair production and muon-nuclear inelastic scattering. In this paper inelastic interactions, i.e., accompanied by particle production, between hadrons and atomic electrons are examined from a similar point of view.

The immediate motivation of this study is the implementation of these inelastic processes into the Monte-Carlo (MC) code CASIM [2]. This code is used, among other things, to evaluate the spatial distribution of the energy deposition for a variety of beam targeting problems. As this study shows, inelastic hadron-electron interactions contribute significantly to such energy deposition. Even though the total cross-section is quite small, the hadron typically loses a large fraction of its energy in such an encounter. For multi-TeV hadrons this makes the "stopping power" of this process exceed that of either bremsstrahlung or pair production. The process bears some resemblance to an inelastic hadron-nucleon collision, since pions, etc., are produced, yet is substantially different due to the much lower average multiplicity (a consequence of the much lower center-of-mass energy) and the presence of the recoil electron. The threshold for pion production off a stationary electron is actually well below 1 TeV (274 GeV for incident protons and 58 GeV for incident pions) but the process gains importance with increasing energy.

The scope of this paper is similar to ref. 1. For each type of outgoing particle, but limited to electrons, pions, and protons,

(i) the inclusive momentum distribution is calculated. For each particle type and for each outgoing momentum (ii) the rms spatial angle between incident and outgoing particle is obtained. Both the momentum distribution and the rms angle as a function of momentum are (iii) suitably parametrized for inclusion into the MC. In addition, (iv) the total cross section and multiplicity are determined as a function of incident energy. Incident particle types are limited to protons and pions.

Based on the above information, a MC simulation of a hadron-electron inelastic event proceeds by selecting type and momentum of the outgoing particle which also determines its rms angle. A random angle is then chosen from a Gaussian with zero mean and standard deviation equal to the rms angle. As commented on in ref. 1, this procedure appears sufficiently accurate for a weighted MC code such as CASIM.

2. Calculation

For hadron production in pe^- interactions there exists a variety of experimental information obtained with e^- beams on p targets. For the contemplated SSC energy of 20 TeV the equivalent e^- energy in the p rest frame is about 11 GeV. There is a substantial amount of data around this energy as well as below it. Data analysis is usually based on the one photon exchange model and is thereby split into two parts: (i) the proton structure function, obtained from the lepton kinematics and (ii) the final state of the virtual photon-hadron interaction. The present problem is then essentially reduced to modelling this information and extracting from it the above mentioned inclusive cross-sections and angles, in the electron rest frame. In computational terms this amounts to evaluating multiple integrals (for the most part numerically) over the kinematical variables of the lepton and, for hadron spectra and angles, over the hadron variables as well.For πe^- interactions no direct experimental information comparable to e^-p exists and so the calculation proceeds mostly by analogy to the proton case.

For the proton structure function, νW_2^p, the Breidenbach and Kuti parametrization [3] is adopted. For R, which relates the structure functions W_1 and W_2, a value 0.18 is assumed when $|q^2| > 1$ GeV^2, where q^2 is the square of the momentum transfer to the lepton, and when $W^2 < 14|q^2|$, where W is the invariant hadron mass. Elsewhere $R=\min(0.18, |q^2|/\nu^2)$ is assumed, with $\nu=(qP)/m$ where (qP) is the four momentum product of the virtual photon and incident hadron of mass m. The pion structure function is taken from work of the CERN-NA3 collaboration [4] on dimuon production in pion-nucleon collisions. Since these measurements are obtained at a mean $|q^2|$ of 25 GeV^2, values of νW_2^π at other q^2 are derived by scaling via the parametrization of the proton structure function:

$$\nu W_2^\pi(q^2,x) = \nu W_2^p(q^2,x) \cdot \nu W_2^\pi(q_0^2,x)/\nu W_2^p(q_0^2,x) \qquad (1)$$

where q_0^2=25 GeV^2 and $x=|q^2|/2m\nu$ is the Bjorken scaling variable. The structure functions plus the atomic form factor and some kinematics suffice to yield the electron momentum spectra and rms angles.

The hadronic final state is modelled as the sum of two contributions: the regular "deep inelastic" process whereby one or more pions are produced plus π's from exclusive ρ^0 production. The latter is introduced separately because it is expressly removed in most experiments which study the hadronic final state and because the two body process $\gamma_V p \to \rho^0 p$, followed by ρ^0 decay, is kinematically quite different from typical non-resonant π production.

In both cases the incident particle is identified in the final state as the "leading particle" and is analyzed separately, i.e., characterized by its own distribution. Leading protons in the deep inelastic process are described by the following parametrization, based on various sources [5]

$$\begin{aligned} \sigma^{-1}E(d^3\sigma/dp^3) &= K(1-x_F)^n \exp(-3p_T^2) \qquad x_F \geq 0 \\ &= K(1+x_F y)\exp(-3p_T^2) \qquad x_F \leq 0 \end{aligned} \qquad (2).$$

In eq. (2) $x_F=p_z/p_z^{max}$ and p_T (in GeV/c) are evaluated in the center of mass frame of the γ_V and incident proton where γ_V points in the positive direction. The exponent n in eq. (2) depends on W:

$$\begin{aligned} n &= 2 - W && W \le 2 \\ &= W - 1 && 2 \le W \le 3.5 \\ &= 2.5 && 3.5 \le W \end{aligned} \qquad (3)$$

as does y

$$\begin{aligned} y &= \min[(4-W)/(4-m_p-2m_\pi),1] && W \le 4 \\ &= 0 && W \ge 4 \end{aligned} \qquad (4)$$

with W in units of GeV. The factor K in eq. (2) follows from normalization, i.e., one proton per interaction. For $\gamma_V p$ the average pion multiplicity (including π^0) is assumed to satisfy

$$\bar{m} = 1.52 \cdot \ln W^2 + 0.705 \qquad (5)$$

with W again in GeV. Conversion of a leading proton into a neutron is not explicitly considered, here or in the parametrization stage, but may readily be introduced in the MC.

The invariant pion production cross section is parametrized by

$$\sigma^{-1} E d^3\sigma/dp^3 = A \cdot \exp(-Bp_T^2 - C_\pm p_z^2) \qquad (6)$$

where C_+ pertains to the γ_V direction in the W rest frame and C_- ($\neq C_+$) to the p direction. The B parameter is expressed in terms of the multiplicity

$$\begin{aligned} B &= 3\bar{m} && \bar{m} < 3.5 \\ &= 21 - 3\bar{m} && 3.5 < \bar{m} < 6.0 \\ &= 3 && 6.0 < \bar{m} \end{aligned} \qquad (7).$$

A and $C_\pm$ follow from conservation of energy and momentum (p_z), minus the leading particle's contribution [eq. (2)], and with eq. (5) fixing the pion multiplicity. All three pion charge states are assumed equally probable. Fig. 1 shows A and $C_\pm$ for incident protons and pions as a function of W^2.

The description of exclusive ρ^0 production relies on the experiment and analysis of Joos et al. [6]. For given q^2 and W, the cross section for exclusive ρ^0 production, expressed as a fraction of the total, is parametrized by

$$F_\rho(q^2,W) = 1.61(W-W_0)^{1/4}\cdot\exp(-|q^2|-2.65(W-W_0)^{1/4}) \qquad (8)$$

where $W_0(\equiv m_p+m_\rho)$, with W in GeV and $|q^2|$ in GeV^2. The differential probability of the reaction $\gamma_V p\rightarrow\rho^0 p$ is assumed to follow

$$P(t,\phi) = k\cdot\exp(-6|t|)/2\pi \qquad (9)$$

where t is the square of the momentum transfer (in GeV^2) and k normalizes $P(t,\phi)$ to unity between the kinematic limits. The ρ-decay distribution is highly simplified from ref. 6:

$$d\sigma/d\cos\theta^\rho_{\pi\gamma} = (3/4)[1 - r^{04}_{00} + (3r^{04}_{00}-1)\cos^2\theta^\rho_{\pi\gamma}] \qquad (10)$$

where $\theta^\rho_{\pi\gamma}$ is the angle between γ_V and either π in the ρ rest frame, and where $r^{04}_{00} = 0.33+0.56|q^2|$ when W<1.85 GeV, while $r^{04}_{00} = 0.2|q^2|$ when W>3 GeV, with $|q^2|$ in GeV^2 and r^{04}_{00} varies linearly in between.

When the electron target is bound in an atom, the process is hindered by an inelastic atomic form factor, though this affects the results only marginally in the energy range of interest here. This form factor is taken from Tsai [7]:

$$G(q^2) = a^4|q^2|^2/(1+a^2|q^2|)^2 \qquad (11)$$

where $a=724\cdot Z^{-2/3}/m_e$, and m_e is the electron mass.

For the $\gamma_V\pi$ interaction, both leading π and produced π (non-resonant or from ρ) are treated entirely similarly to $\gamma_V p$, except for the p-π mass difference. As a consequence limits on W, etc., as occur in eqs. (3)-(7), and pertaining specifically to the proton case, need be adjusted.

3. Results

In this section parametrizations of cross sections and angles are described and compared with results calculated in the manner of sec. 2. Matters are concluded with some general results on total cross sections, multiplicities, energy loss and angular diffusion.

The cross section parametrizations are not explicitly normalized. For comparison with direct calculation, the form $\sigma^{-1}d\sigma/dp$ is adopted which fixes the integral over all outgoing momenta, p, to unity for both electron and leading particle, and to $\bar{m}$ for the produced particles. The σ and $\bar{m}$ needed for absolute normalization are given separately. All parametrizations presented here are for the case of a stationary free electron. The atomic form factor correction is quite small and its effect on total cross sections is discussed below. Its effect on the shape of the hadron spectra is negligible. Corrections to the electron spectra may be applied directly from eq. (11) using $E_{e'}=|q^2|/2m_e+m_e$.

To simplify matters the deep inelastic and exclusive ρ^0 contributions are always combined. The parametrizations of $d\sigma/dp$ (but not of the angles) are constrained to be in a form easy to sample from in a MC. In all formulae below masses, momenta, and energies are expressed in GeV.

3.1. Electron.

The electron momentum spectrum for incident protons is well represented by

$$\begin{aligned}
\sigma^{-1}d\sigma/dp_e &= k_1(v/v_1)^m && v_0 \le v \le v_1 \\
&= k_2 && v_1 \le v \le v_2 \\
&= k_2(v_2/v)^{1.034} && v_2 \le v \le v_3 \\
&= k_3(v_3/v)^n && v_3 \le v \le v_4 \\
&= k_4[\exp(-15v)+1.23\cdot10^{-3}p_0\exp(-53v)] && v_4 \le v \le v_5 \qquad (12)
\end{aligned}$$

and zero elsewhere. Here $v \equiv p/p_0$ is the electron momentum expressed as a fraction of the incident proton momentum, p_0. The k_i follow from continuity and normalization; $m=7/r_p^{0.2}$ with $r_p=(1-p_{th}^2/p_0^2)$ where p_{th} is the threshold momentum (274 GeV for protons) and $n=1.4+0.0023\sqrt{p_0}$. The v boundaries are: $v_0=0.25/(p_0^{2.06}r_p^{0.7})$, $v_1=1.06v_0p_0^{0.05}$, $v_2=0.15/(p_0^2r_p)^{0.89}$, $v_3=3.0/p_0^{0.7}$, $v_4=0.04$, $v_5=1-213r_p^{0.34}/p_0^{0.84}$. Fig. 2(a) compares the parametrization of eqs. (12) and (13) with direct calculation as outlined in sec. 2.

The rms angles between outgoing electron and incident proton are parametrized as follows:

$$\begin{aligned}
\langle\theta_e^2\rangle^{1/2} &= (1.31-31p_0^{-0.57})\cdot(v/v_b)^i && v_a \le v \le v_b \\
&= k_2 && v_b \le v \le v_c \\
&= k_2\cdot(v_c/v)^{1/2} && v_c \le v \le v_d \\
&= k_4\cdot(v_d/v)^j && v_d \le v \le v_e \\
&= k_5\cdot[\exp(-2.6v)+2.3\exp(-18v)] && v_e \le v \le v_f \qquad (13)
\end{aligned}$$

with $i=0.7/\sqrt{r_p}$, $j=0.54/r_p^{0.3}$, $v_a=0.23/(p_0^{2.05}r_p^{0.72})$, $v_b=0.45v_ap_0^{0.23}$, $v_c=0.0040/(p_0^{1.2}r_p)$, $v_d=0.007$, $v_e=0.07$ and $v_f=v_5$ where v_5 is from eq. (12). Fig. 2(b) compares $\langle\theta_e^2\rangle^{1/2}$ from eq. (13) with direct calculation.

The parametrization of electron momentum spectra and rms angles from collisions with incident pions follows closely that of protons:

$$\begin{aligned}
\sigma^{-1}d\sigma/dp_e &= k_1(v/v_1)^i && v_0 \le v \le v_1 \\
&= k_2 && v_1 \le v \le v_2 \\
&= k_2(v_2/v)^{1.07} && v_2 \le v \le v_3 \\
&= k_3(v_3/v)^j && v^3 \le v \le v_4 \\
&= k_4[\exp(-\alpha v)+500p_0^{0.17}\exp(-\beta v)] && v_4 \le v \le v_5 \qquad (14)
\end{aligned}$$

where $i=7/r_\pi^{0.3}$ with $r_\pi=(1-p_{th}^2/p_0^2)$, but p_{th} is now the pion threshold ($\simeq$57 GeV/c), $j=1.3+6.7\cdot10^{-6}p_0$, $\alpha=0.032p_0^{0.52}$, $\beta=18.4p_0^{0.08}$,

$v_0=0.027/(p_0^2 r_\pi^{0.7})$, $v_1=1.78v_0$, $v_2=0.038/(p_0^2 r_\pi)^{0.89}$, $v_3=0.3/p_0^{0.6}$, $v_4=4.3/\sqrt{p_0}$, $v_5=1-47/p_0^{0.93}$.

The rms angle of the electron as a function of v for the eπ case is parametrized as:

$$\begin{aligned}
\langle\theta_e^2\rangle^{1/2} &= (1.5-6.0/p_0^{0.38})\cdot(v/v_b)^j && v_a \le v \le v_b \\
&= k_2 && v_b \le v \le v_c \\
&= k_2\cdot(v_c/v)^{1/2} && v_c \le v \le v_d \\
&= k_4\cdot[\exp(-2.6v)+1.4\exp(-20v)] && v_d \le v \le v_e \qquad (15)
\end{aligned}$$

where $j=0.88/\sqrt{r_\pi}$, $v_a=v_0$, $v_b=1.1p_0^{0.13}v_a$, $v_c=0.0017/(p_0^2 r_\pi)^{0.56}$, $v_d=0.07$, $v_e=v_5$ and v_0, v_5 refer to eq. (14). Fig. 3 compares $\sigma^{-1}d\sigma/dp_e$ and $\langle\theta_e^2\rangle^{1/2}$ obtained by direct calculation with eqs. (14) and (15).

3.2. Leading particle.

The momentum spectrum for leading protons is represented by

$$\begin{aligned}
\sigma^{-1}d\sigma/dp_p &= k_1\cdot v'^m && v_{min} \le v \le v_1 \\
&= k_2\cdot[(1-v')/(1-v_1')]^n && v_1 \le v \le v_{max} \qquad (16)
\end{aligned}$$

where $v'=(v-v_{min})/(v_{max}-v_{min})$, and v_{min}, v_{max} are the kinematic limits for single pion production; $m=16.4/p_0^{0.22}$, $n=22.5/p_0^{0.23}$ and the boundary $v_1=0.874-2.67\cdot10^{-6}p_0\sqrt{r_p}$.

The rms angle between leading p and incident p follows

$$\begin{aligned}
\langle\theta_p^2\rangle^{1/2} &= 2.3\cdot10^{-4}v'^i && 0 \le v' \le v_a' \\
&= k_2\cdot v'^j && v_a' \le v' \le v_b' \\
&= k_3\cdot[(1-v')/(1-v_b')]^m && v_b' \le v' \le v_c' \\
&= k_4\cdot[(1-v_c')/(1-v')]^{0.26} && v_c' \le v' \le v_d' \\
&= k_5\cdot[(1-v')/(1-v_d')]^{0.28} && v_d' \le v' \le 1 \qquad (17)
\end{aligned}$$

where $i=38.2/p_0^{0.8}$, $j=-0.75+19.1/\sqrt{p_0}$, and $m=2.85/p_0^{0.08}$. The v boundaries are $v'_a=0.0089[r_p(-1+3.1\cdot10^4/p_0)]^{1/2}$, $v'_b=0.18+3.1(r_p/p_0)^{0.3}$, $v_c=0.874-3.2\cdot10^{-6}(p_0\sqrt{r_p})$ and $v'_d=0.95-30/(p_0\sqrt{r_p})$. The fits are shown in fig. 4.

The leading pion momentum spectrum is approximated by:

$$\begin{aligned}
\sigma^{-1}d\sigma/dp_\pi &= k_1\cdot v'^{i} && 0 \le v' \le v'_1\\
&= k_2\cdot\exp[(2.1+49/p_0^{0.36})v'] && v'_1 \le v' \le v'_2\\
&= k_3\cdot\exp(-8.8v')\cdot p_0^{1.1v'} && v'_2 \le v' \le v'_3\\
&= k_4\cdot\exp(-8.1v')\cdot p_0^{2.2v'} && v'_3 \le v' \le v'_4\\
&= k_5\cdot[(1-v')/(1-v'_4)]^{j} && v'_4 \le v' \le 1 \qquad (18)
\end{aligned}$$

where $i=44/p_0^{0.47}$, $j=14.3/p_0^{0.28}$, $v'_1=0.26$, $v_2=0.5$, $v'_3=0.74$ and $v'_4=0.74+2.6/\sqrt{p_0}$.

The rms angle of the leading pion is fitted by:

$$\begin{aligned}
\langle\theta_\pi^2\rangle^{1/2} &= 0.25v'^{j}/p_0^{0.95} && 0 \le v' \le v'_a\\
&= k_2\cdot\exp(-2.2p_0^{0.075}v') && v'_a \le v' \le v'_b\\
&= k_3\cdot\exp(0.92v') && v'_b \le v' \le v'_c\\
&= k_4\cdot[(1-v')/(1-v'_c)]^{m} && v'_c \le v' \le 1 \qquad (19)
\end{aligned}$$

where $j=-0.9+15.6/\sqrt{p_0}$, $m=0.69/p_0^{0.13}$, $v'_a=0.14+7200/p_0^2$, $v_b=0.5$, and $v'_c=0.55+1.15\cdot10^{-3}\sqrt{p_0}$. Fig. 5 compares this with direct calculation.

3.3 Produced Pions.

For pions produced by incident protons the momentum spectra are parametrized as:

$$\begin{aligned}
\sigma^{-1}d\sigma/dp_\pi &= k_1\cdot(v')^{2.1} && v_{min} \le v \le v_1 \\
&= k_2\cdot(v'/v_1')^{i} && v_1 \le v \le v_2 \\
&= k_3\cdot(v'/v_2')^{j} && v_2 \le v \le v_3 \\
&= k_4\cdot\exp(-19.8v'/p_0^{0.12}) && v_3 \le v \le v_4 \\
&= k_5\cdot\exp(-14.3v') && v_4 \le v \le v_5 \\
&= k_6\cdot[(1-v')/(1-v_5')]^{m} && v_5 \le v \le v_{max} \qquad (20)
\end{aligned}$$

where $i=2.0/p_0^{0.05}$, $j=146/(p_0^2 r_p)^{0.3}$, $m=11.5-42/p_0^{0.27}$, $v_1=33/p_0$, $v_2=9.3/p_0^{0.75}$, $v_3=0.13$, $v_4=0.26r_p^{0.38}$, $v_5=v_4+8.7\cdot10^{-9}p_0^2$.

The rms angle of the produced π is represented by

$$\begin{aligned}
\langle\theta_\pi^2\rangle^{1/2} &= 7.4\cdot10^{-4}p_0^{0.32}r_p^{0.66}v'^{0.35} && v_{min} \le v \le v_a \\
&= k_2 && v_a \le v \le v_b \\
&= k_2\cdot(v_b'/v')^{0.56} && v_b \le v \le v_c \\
&= k_3\cdot(v_c/v) && v_c \le v \le v_d \\
&= k_4\cdot(v/v_d)^{i} && v_d \le v \le v_e \\
&= k_5\cdot[(1-v')/(1-v_e')]^{0.54} && v_e \le v \le v_{max} \qquad (21)
\end{aligned}$$

where $i=-1+26/p_0^{0.44}$, $v_a=24/p_0^{0.96}$, $v_b'=49(r_p^{0.27}p_0)$, $v_c=3.5r_p^{0.25}/\sqrt{p_0}$, $v_d=0.13$, and $v_e=0.144+5.0\cdot10^{-6}p_0$. The fits are illustrated in fig. 6.

Pions produced by an incident pion have a momentum distribution approximated by

$$\begin{aligned}
\sigma^{-1}d\sigma/dp_\pi &= k_1\cdot v'^{i} && 0 \le v' \le v_1' \\
&= k_2\cdot(1-v')^{j} && v_1' \le v' \le v_2' \\
&= k_3\cdot(1-v')^{m} && v_2' \le v' \le 1 \qquad (22)
\end{aligned}$$

where $i=-1+10.2r_\pi^{4.6}/p_0^{0.22}$, $j=0.38p_0^{0.15}$, $m=2.8p_0^{0.01}$, $v_1'=0.5/p_0^{0.02}$, $v_2'=0.44p_0^{0.03}$.

The rms angle of these π obeys

$$\begin{aligned}
\langle\theta_\pi^2\rangle^{1/2} &= 0.33\cdot v'^{i}/(p_0 r_\pi^{13}) && 0 \le v' \le v'_a \\
&= k_2\cdot\exp(-2.7p_0^{0.031}v') && v'_a \le v' \le v'_b \\
&= k_3\cdot\exp[-(1.38-24/\sqrt{p_0})v'] && v'_b \le v' \le v'_c \\
&= k_4\cdot[(1-v')/(1-v'_c)]^j && v'_c \le v' \le 1 \qquad (23)
\end{aligned}$$

where $i=17.3/\sqrt{p_0}-1$, $j=1.57/p_0^{0.2}$, $v'_a=0.043p_0^{0.17}$, $v_b=0.52$ and $v'_c=0.7$. Parametrizations and direct calculation are compared in fig. 7.

3.4 General.

Fig. 8 presents the total inelastic cross section on a stationary free electron, for protons as well as for pions, along with the average pion multiplicity per event. These quantities are needed to normalize the parametrizations. Also shown is the fraction of the total cross section which is exclusive ρ production. It is seen that σ_{tot}, while not very large, is still quite significant amounting to a few millibarn per atom for high Z species in the upper part of the energy range explored here (compared to an inelastic nuclear cross section of ~1.5-2 barn).

The effect of the atomic form factor on the total cross section is displayed in fig. 9. Below 30 TeV it is still a small effect, essentially neglible within the accuracy of the model. But the trend of fig. 9 indicates that the effect becomes important at somewhat higher energies.

Fig. 10 shows how the lab energy of the incident particle is divided among the final state particles. Leading protons retain, on average, the major fraction of their energy but leading pions appear to lose more than half of theirs. The electron recoil energy, while small on a fractional basis, is nonetheless in the multi-GeV range.

The average stopping power (dE/dx) of the inelastic process is compared to that of other processes (from ref. 1) in fig. 11 for protons on beryllium and lead. This illustrates the Z dependence. For both materials the inelastic process becomes the largest contributor to dE/dx above a few TeV but it is more dominant in beryllium. This follows because pair production and bremsstrahlung proceed mainly coherently off nuclei and are therefore more competitive for high Z materials. The dE/dx for protons is compared with that of pions for the case of iron in fig. 12. Again the inelastic process is the largest above a few TeV and is seen to more dominant for the proton case. This is a consequence of the lighter pion mass which leads to a larger contribution from the competing processes.

Fig. 13 shows the averaged (over all outgoing momenta) rms angle in bulk matter for the inelastic process as well as for the other processes (also from ref. 1) again for protons on beryllium and lead. Fig. 14 displays the same angles for protons and for pions on iron. In all cases the inelastic process appears to be the largest contibutor to the angular diffusion as well, though not quite as prominently as for dE/dx. Both rms angle and dE/dx calculations include the effect of the atomic form factor.

In conclusion, it appears then that the preceding results bear some interesting consequences for the spatial distribution of the energy deposition along the path of, e.g., a 20 TeV proton beam striking a thick target. The inelastic process is important both for energy loss and angular diffusion of the beam and must be included in MC (or other) calculations to obtain quantitative results in this and similar applications.

We wish to thank L. Teng and F. Turkot for reading the manuscript.

References

[1] A. Van Ginneken, Energy Loss and Angular Characteristics of High Energy Electromagnetic Processes, Nucl. Inst. Meth. A251 (1986) 21.

[2] A. Van Ginneken, Fermilab-FN-272 (1975).

[3] M. Breidenbach and J. Kuti, Phys. Lett., 41B (1972) 345.

[4] J. Badier et al., Z. Phys. C18 (1983) 281; see also E. L. Berger, in Particles and Fields-1982, W. E. Caswell and G. A. Snow, Eds., AIP, New York (1982), p312ff.

[5] H. Ackermann et al., Nucl. Phys. B120 (1977) 365; J. C. Alder et al., Nucl. Phys. B46 (1972) 415; L. Ahrens et al., Phys. Rev. D9 (1974) 1894; C. J. Bebek et al., Phys. Rev. Lett. 32 (1974) 27; C. J. Bebek et al., Phys. Rev. Lett. 34 (1975) 1115; C. J. Bebek et al., Phys. Rev. D15 (1977) 3077; A. Browman et al., Phys. Rev. Lett. 37 (1976) 651; A. Browman et al., ibid., 974; P. H. Garbincius et al., Phys. Rev. Lett. 32 (1974) 328; B. Gibbard et al., Phys. Rev. D11 (1975) 2367; W. A. Loomis et al., Phys. Rev. D19 (1979) 2543.

[6] P. Joos et al., Nucl. Phys. B113 (1976) 53.

[7] Y. S. Tsai, Rev. Mod. Phys. 46 (1974) 815.

Figure Captions

Fig. 1. (a) Parameters A, C_+ and C_- of eq. (6) describing pion production by incident protons in the $\gamma_V p$ frame as a function of W^2, the square of the invariant mass of the hadronic system.

(b) Ditto for pion production by incident pions in the $\gamma_V \pi$ frame.

Fig. 2. (a) Inclusive electron recoil distribution for incident protons as a function of v, the lab momentum of the electron as a fraction of the incident momentum. In figs. 2-7 the symbols (see legend) represent direct calculation (from sec. 2) and the curves (see legend) are empirical fits (from sec. 3).

(b) Rms angle of electron with respect to incident proton as a function of v.

Fig. 3. (a) Inclusive electron recoil distribution for incident pions as a function of v.

(b) Rms angle of electron with respect to incident pion as a function of v.

Fig. 4. (a) Inclusive leading proton distribution as a function of v.

(b) Rms angle of leading proton with respect to incident proton as a function of v.

Fig. 5. (a) Inclusive leading pion distribution as a function of v.

(b) Rms angle of leading pion with respect to incident pion as a function of v.

Fig. 6. (a) Inclusive produced pion distribution for incident protons as a function of v.

(b) Rms angle of produced pion with respect to incident proton as a function of v.

Fig. 7. (a) Inclusive produced pion distribution for incident pions as a function of v.

(b) Rms angle of produced pion with respect to incident pion as a function of v.

Fig. 8. Total cross section in mb for a stationary free electron (right scale), percentage of total cross section which is exclusive ρ^0 production, and average produced pion multiplicity (left scale) as a function of the incident energy in TeV (a) for incident protons, (b) for incident pions.

Fig. 9. Reduction of total cross section due to inelastic form factor for beryllium, iron, and lead as a function of incident energy in TeV, expressed as a fraction of the total cross section (a) for incident protons and (b) for incident pions.

Fig. 10. Fraction of incident energy carried off by recoil electron (right scale), by leading particle and by produced particles (left scale) as a function of incident energy in TeV (a) for incident protons and (b) for incident pions.

Fig. 11. Proton stopping power as a function of energy in TeV due to various processes in (a) berryllium and (b) lead. Legend: CL, collision energy losses; pp, pair production; BR, bremsstrahlung; Inelastic, accompanied by particle production.

Fig. 12. Stopping power in iron as a function of energy in TeV due to various processes for (a) protons and (b) pions. Legend: see fig. 11.

Fig. 13. Rms angle in bulk matter as a function of energy in TeV due to various processes in (a) berryllium and (b) lead. Legend: see fig. 11.

Fig. 14. Bulk matter rms angle in iron as a function of energy in TeV due to various processes for (a) protons and (b) pions. Legend: see fig. 11.

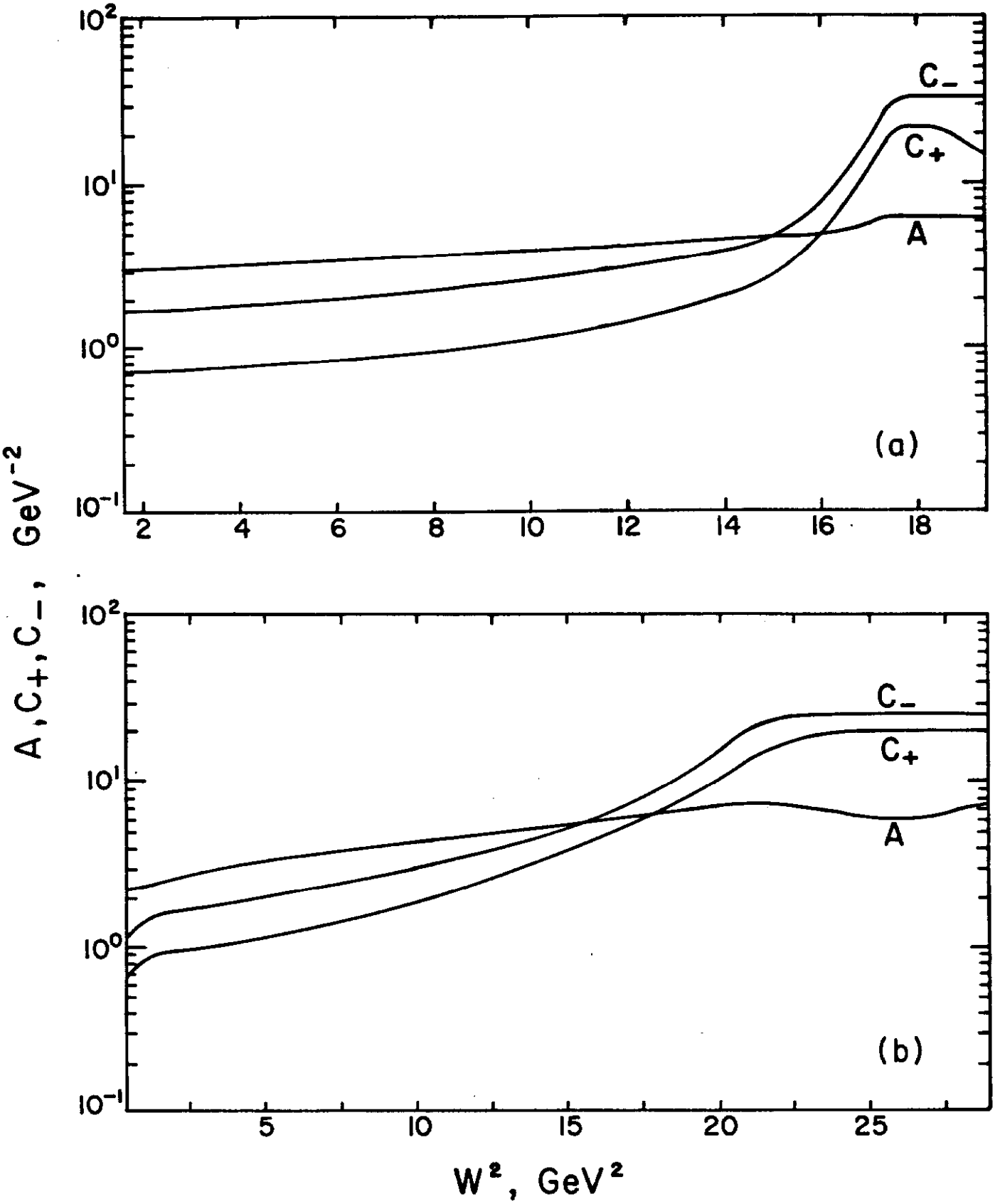
10^2
10^1
10^0
10^{-1}
C_
C+
A
(a)
2
4
6
8
10
12
14
16
18
A, C+, C_, GeV^{-2}
10^2
10^1
10^0
10^{-1}
C_
C+
A
(b)
5
10
15
20
25
W^2, GeV^2

Fig. 1

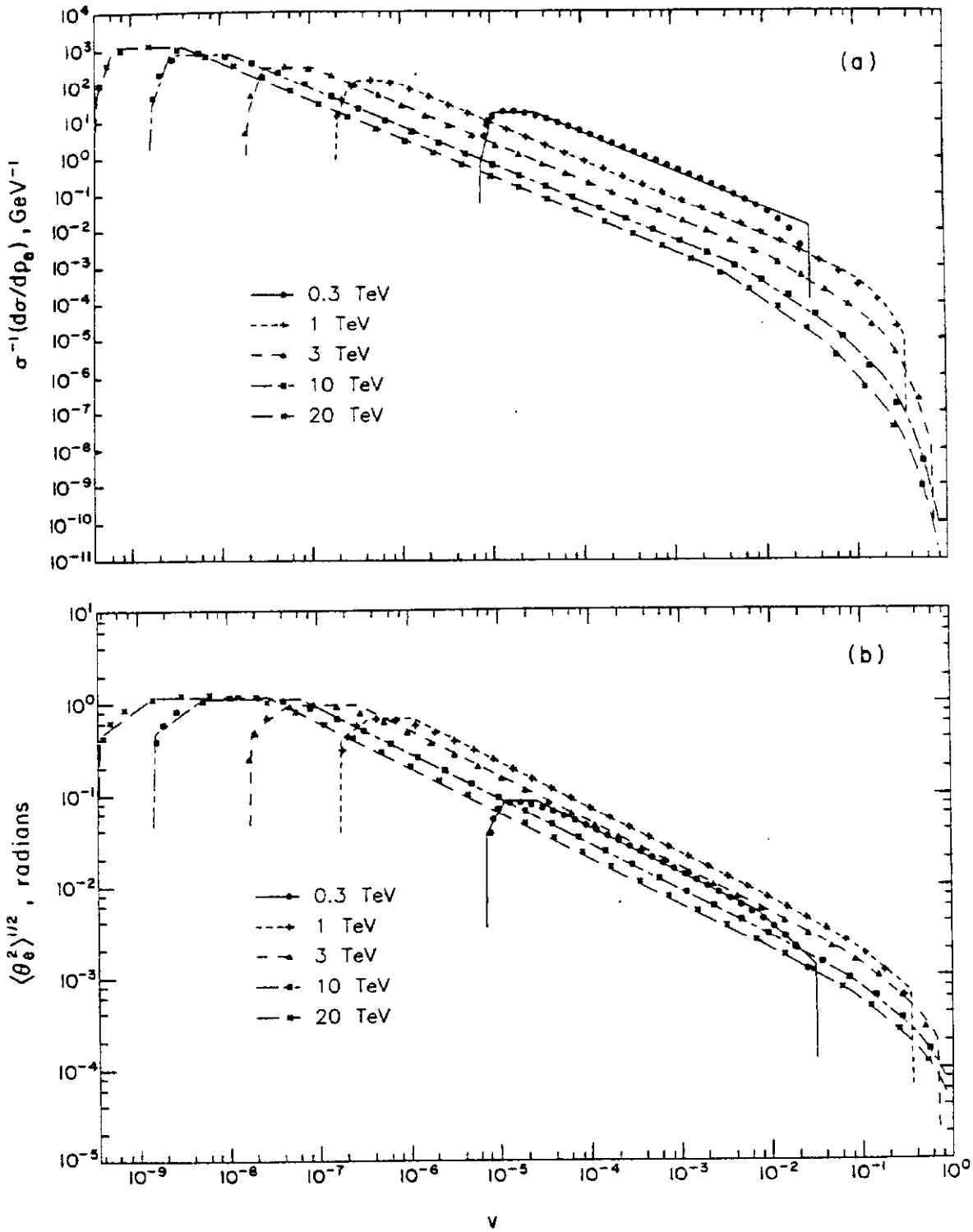
(a)
$\sigma^{-1}(d\sigma/dp_\theta)$, GeV^{-1}
0.3 TeV
1 TeV
3 TeV
10 TeV
20 TeV
(b)
$\langle\theta_\theta^2\rangle^{1/2}$, radians
0.3 TeV
1 TeV
3 TeV
10 TeV
20 TeV
v

Fig. 2

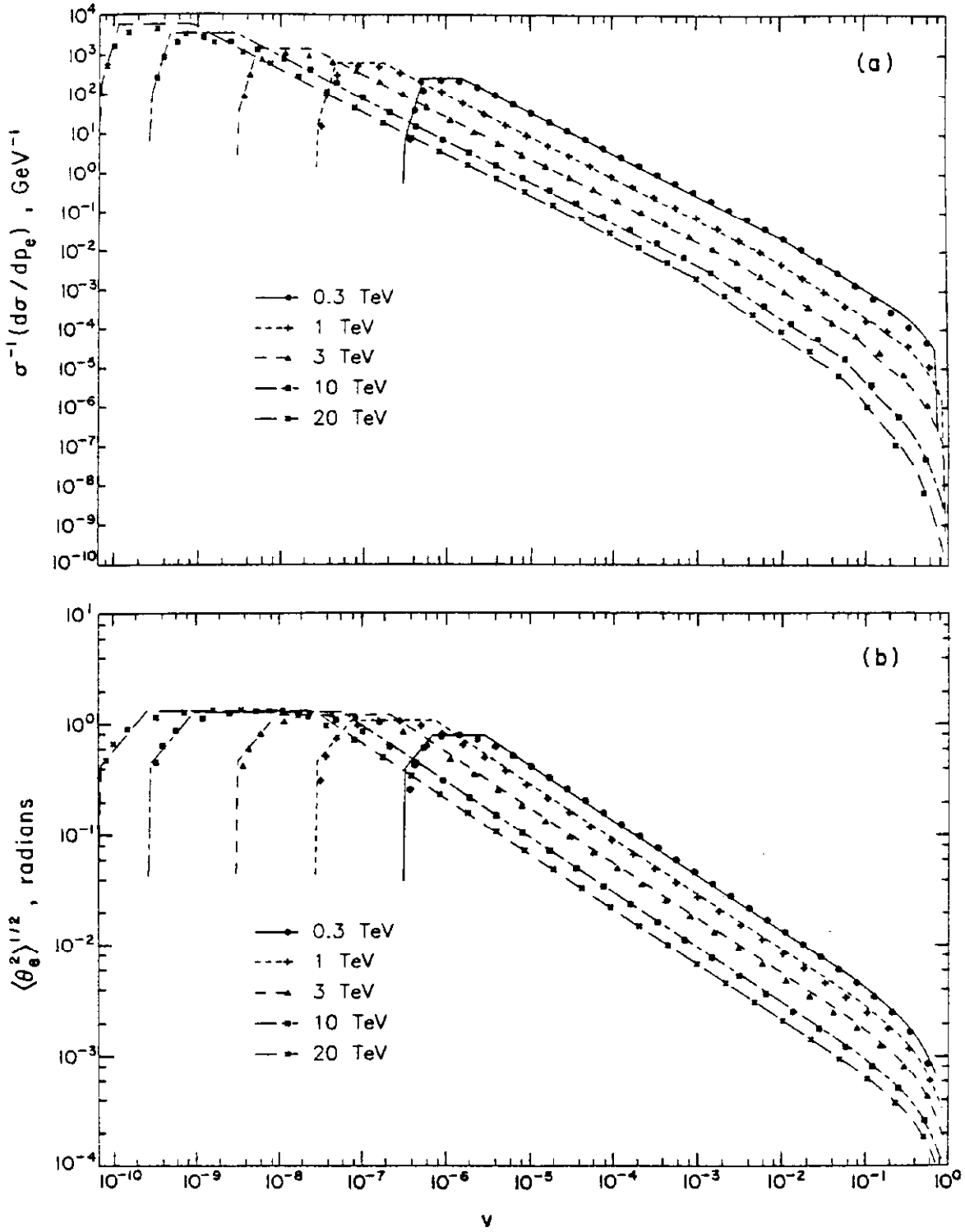
(a)
$\sigma^{-1}(d\sigma/dp_e)$, GeV^{-1}
0.3 TeV
1 TeV
3 TeV
10 TeV
20 TeV
(b)
$\langle\theta_e^2\rangle^{1/2}$, radians
0.3 TeV
1 TeV
3 TeV
10 TeV
20 TeV
v

Fig. 3

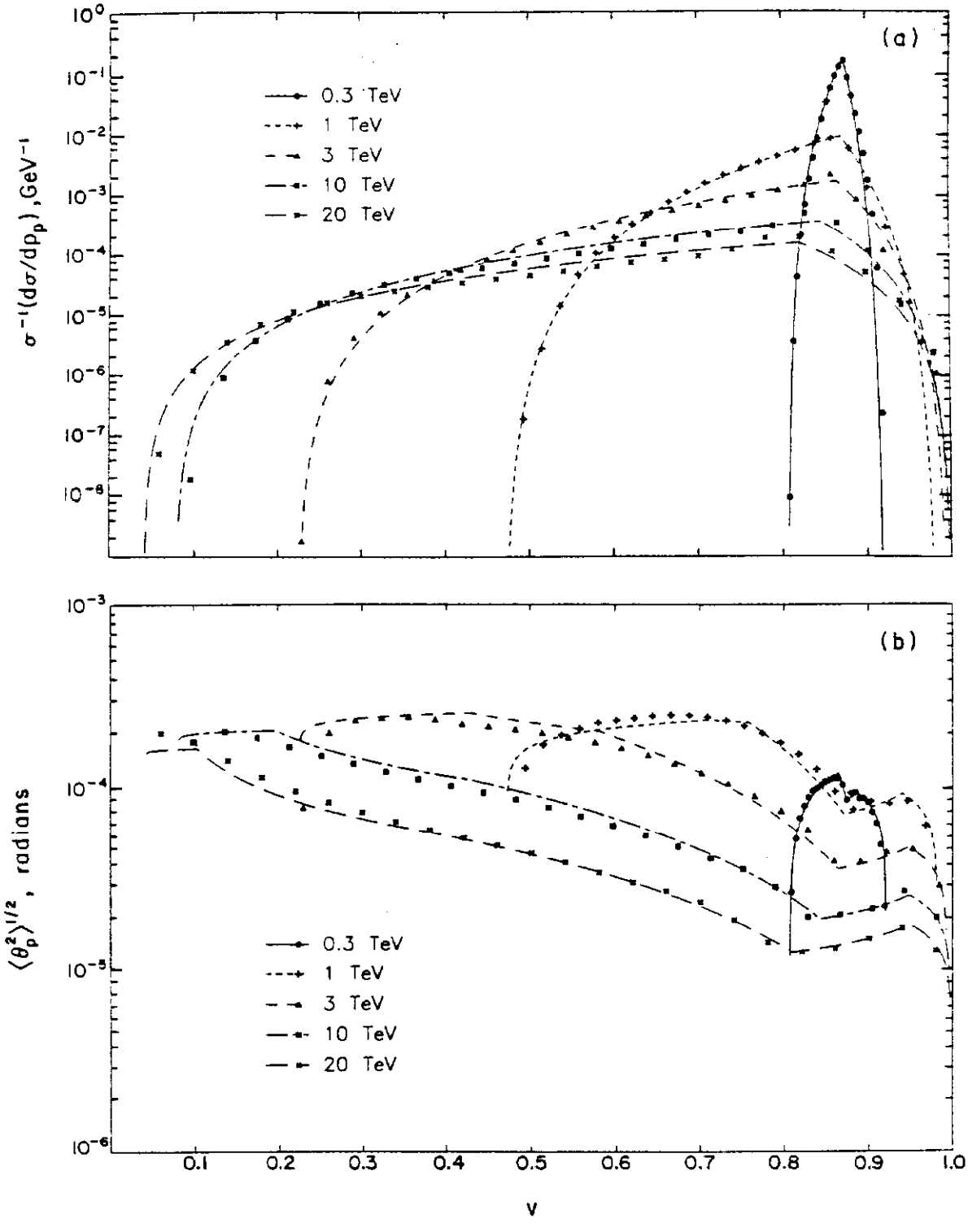
(a)
0.3 TeV
1 TeV
3 TeV
10 TeV
20 TeV
$\sigma^{-1}(d\sigma/dp_p)$, GeV^{-1}
(b)
$\langle\theta_p^2\rangle^{1/2}$, radians
v

Fig. 4

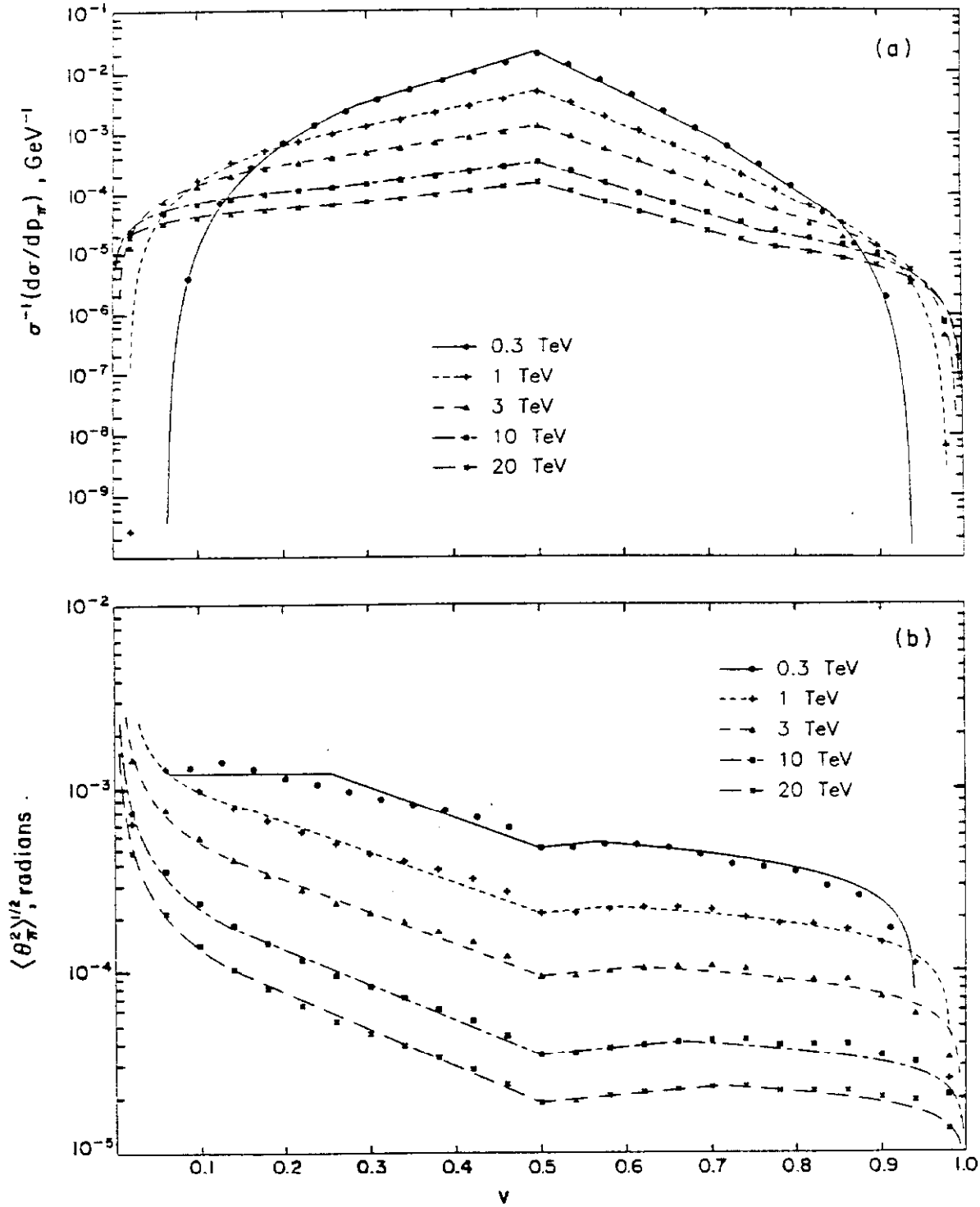
(a)
$\sigma^{-1}(d\sigma/dp_\pi)$, GeV^{-1}
0.3 TeV
1 TeV
3 TeV
10 TeV
20 TeV
(b)
$\langle\theta_\pi^2\rangle^{1/2}$, radians
0.3 TeV
1 TeV
3 TeV
10 TeV
20 TeV
v

Fig. 5

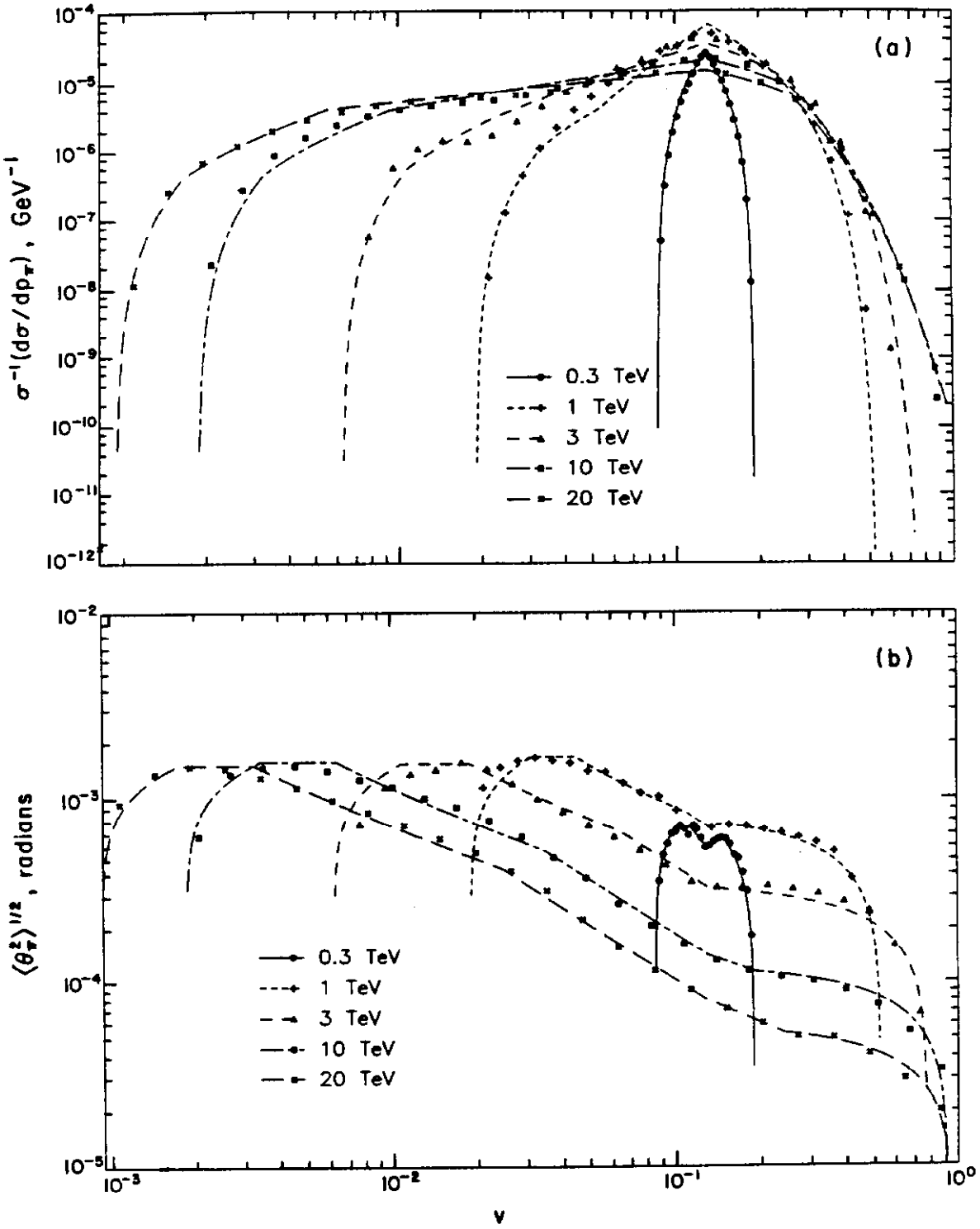
(a)
$\sigma^{-1}(d\sigma/dp_\pi)$, GeV^{-1}
0.3 TeV
1 TeV
3 TeV
10 TeV
20 TeV
(b)
$\langle\theta_\pi^2\rangle^{1/2}$, radians
0.3 TeV
1 TeV
3 TeV
10 TeV
20 TeV
v

Fig. 6

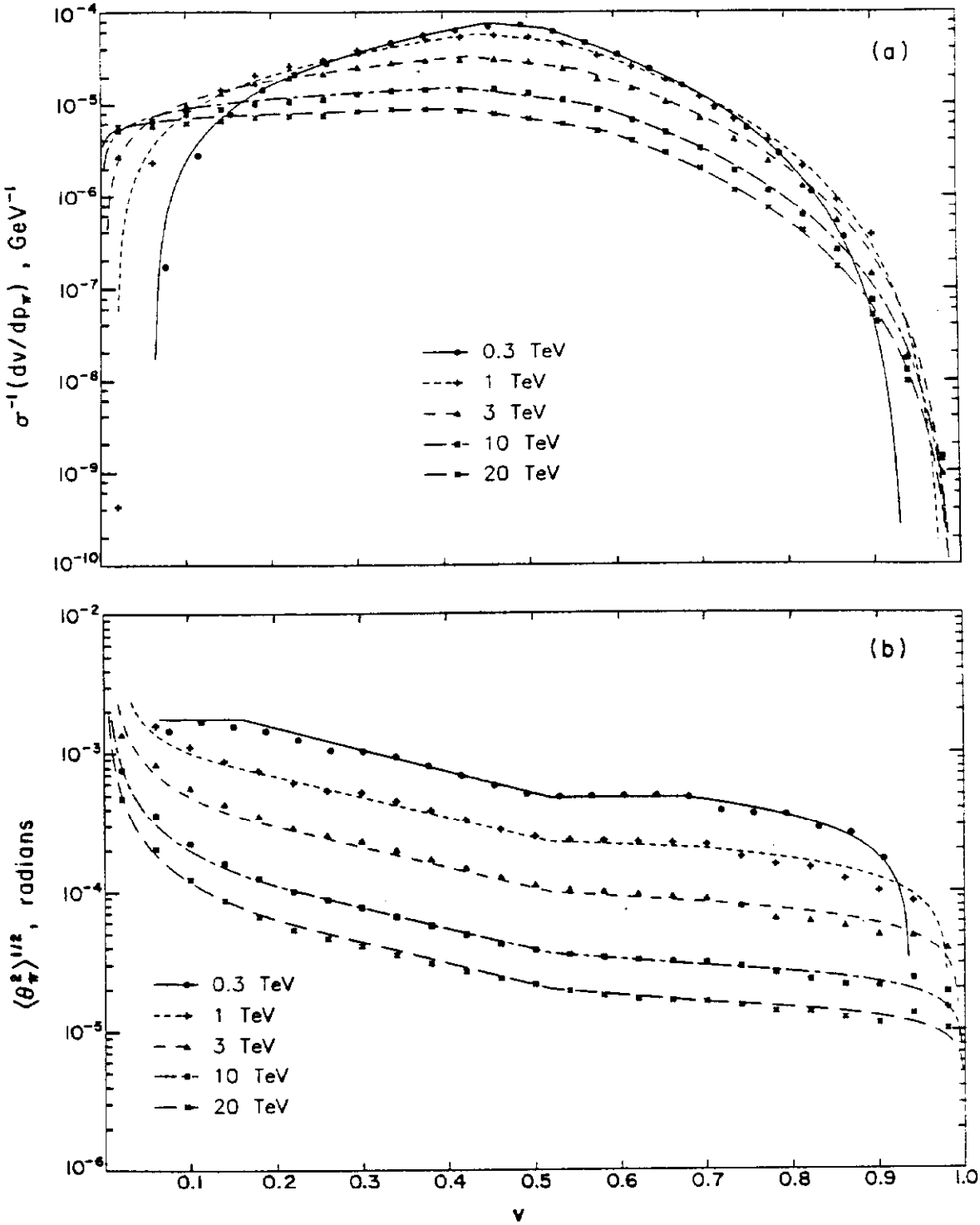
(a)
$\sigma^{-1}(d\nu/dp_\pi)$, GeV^{-1}
0.3 TeV
1 TeV
3 TeV
10 TeV
20 TeV
(b)
$\langle\theta_\pi^2\rangle^{1/2}$, radians
0.3 TeV
1 TeV
3 TeV
10 TeV
20 TeV
ν

Fig. 7

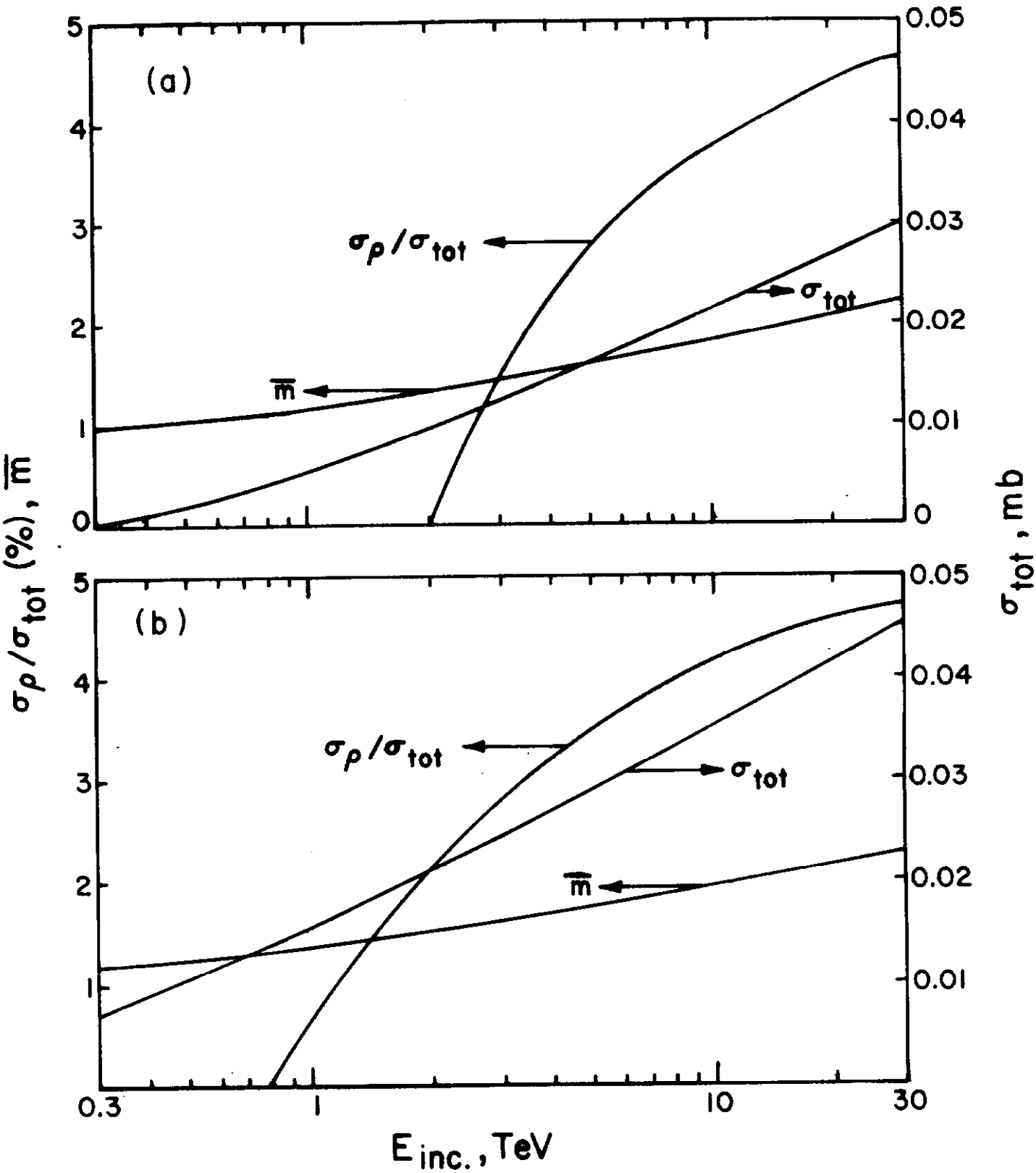
(a)
(b)
σ_ρ/σ_{tot}
σ_{tot}
$\bar{m}$
σ_ρ/σ_{tot} (%), $\bar{m}$
σ_{tot}, mb
$E_{inc.}$, TeV
0.3
1
10
30

Fig. 8

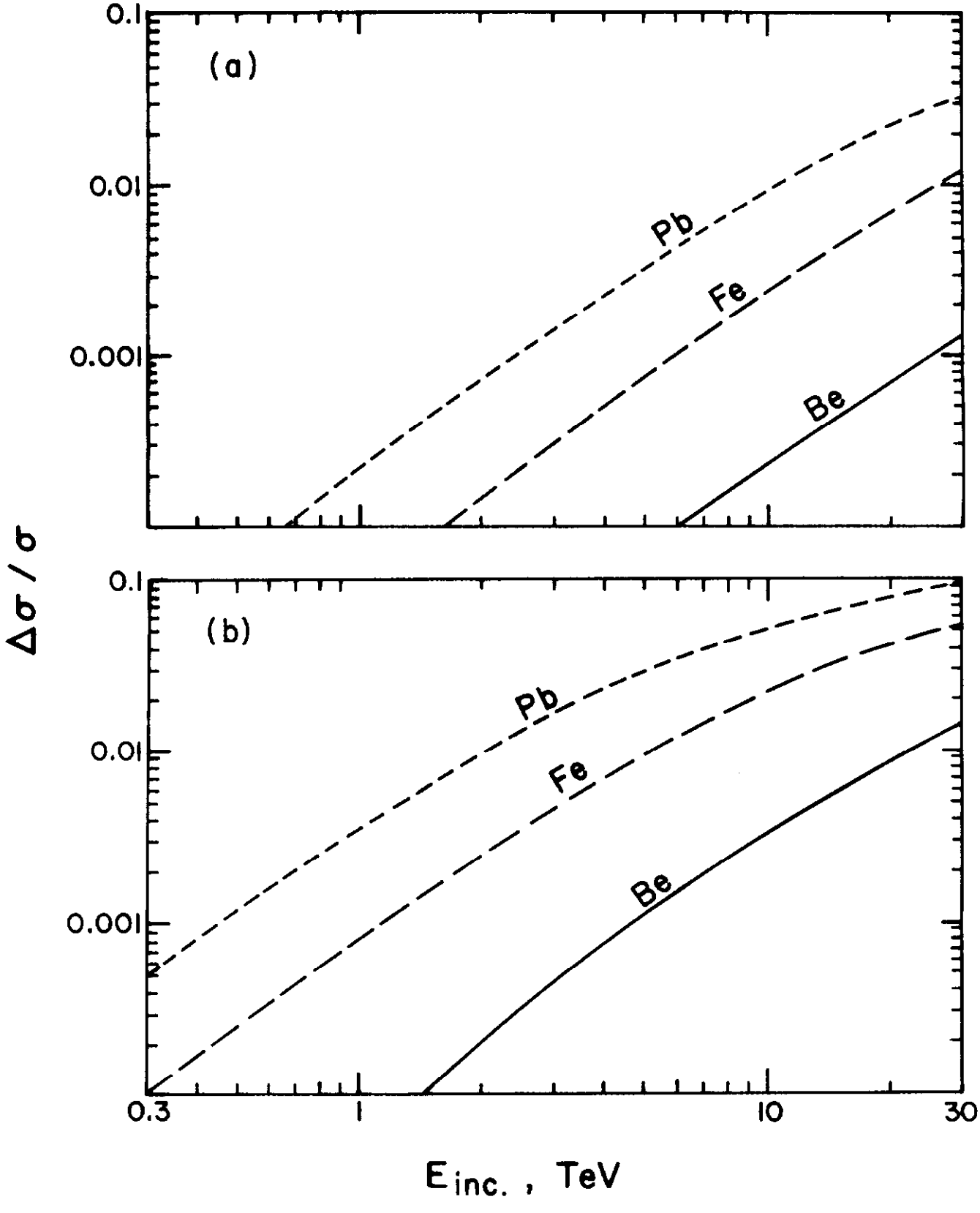

Fig. 9

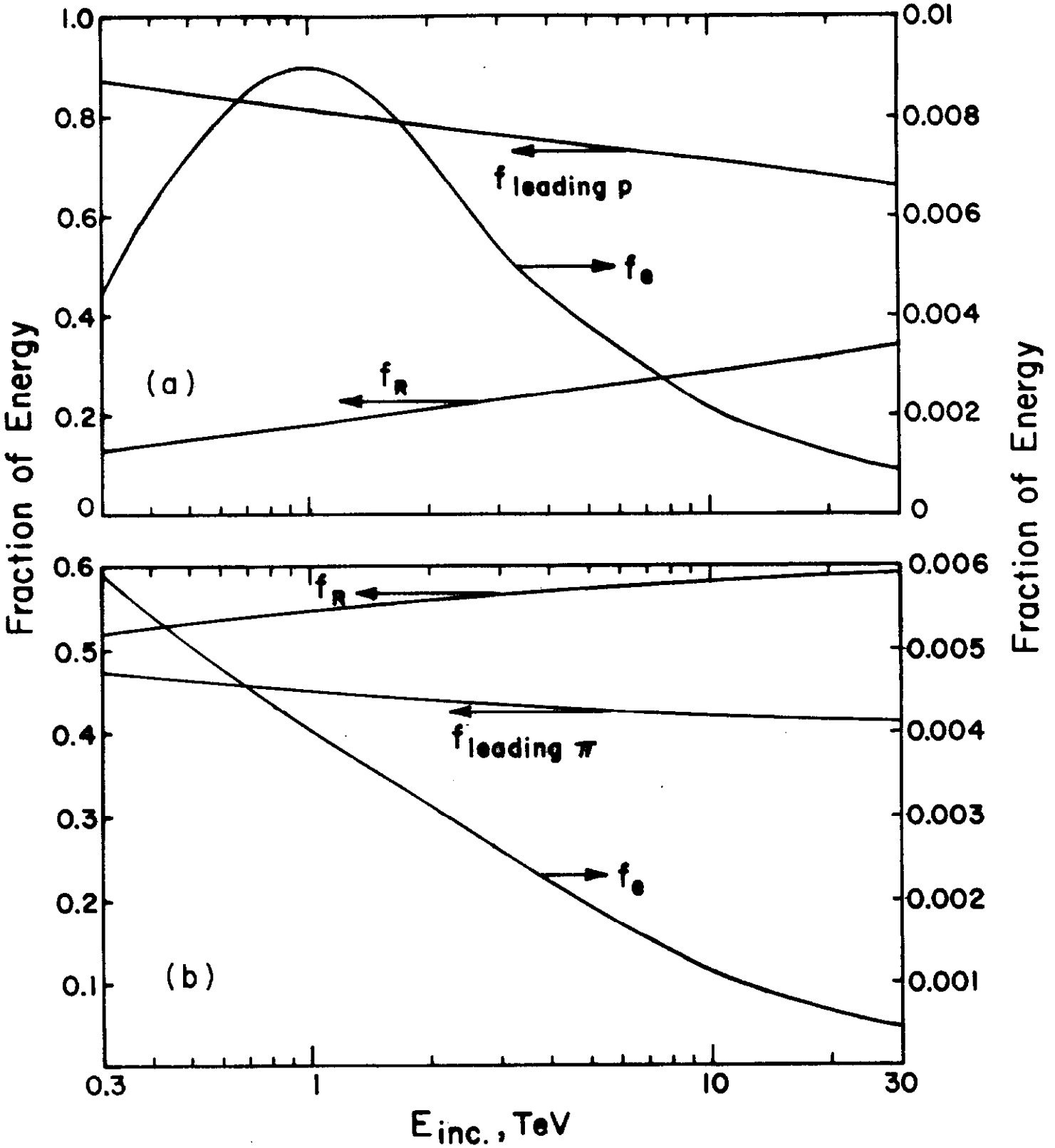
1.0
0.8
0.6
0.4
0.2
0
0.01
0.008
0.006
0.004
0.002
0
$f_{leading\ p}$
f_e
f_R
(a)
Fraction of Energy
0.6
0.5
0.4
0.3
0.2
0.1
0.006
0.005
0.004
0.003
0.002
0.001
f_R
$f_{leading\ \pi}$
f_e
(b)
0.3
1
10
30
$E_{inc.}$, TeV

Fig. 10

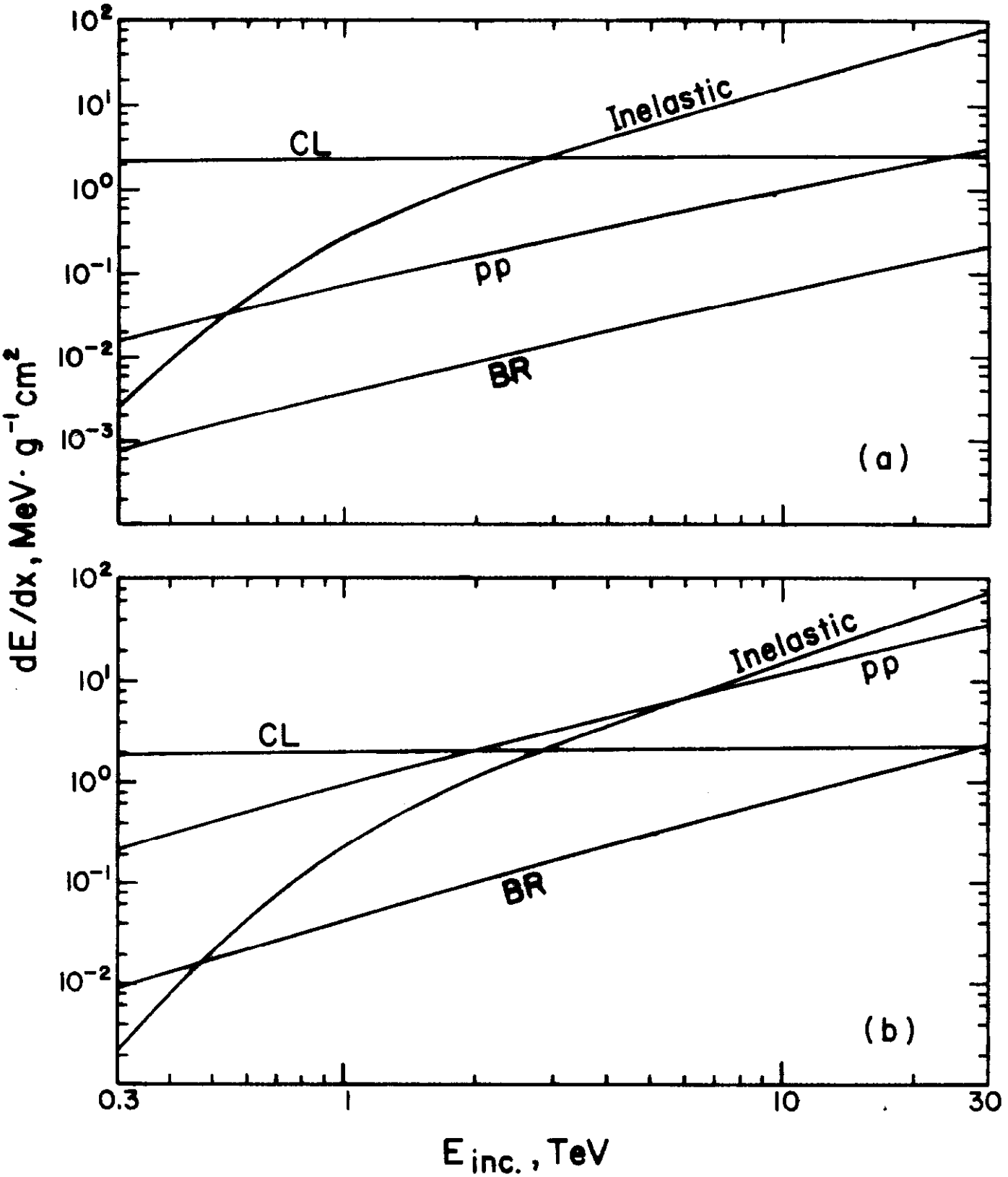
Inelastic
CL
pp
BR
(a)
Inelastic
pp
CL
BR
(b)
dE/dx, MeV·g⁻¹cm²
E inc., TeV
0.3
1
10
30

Fig. 11

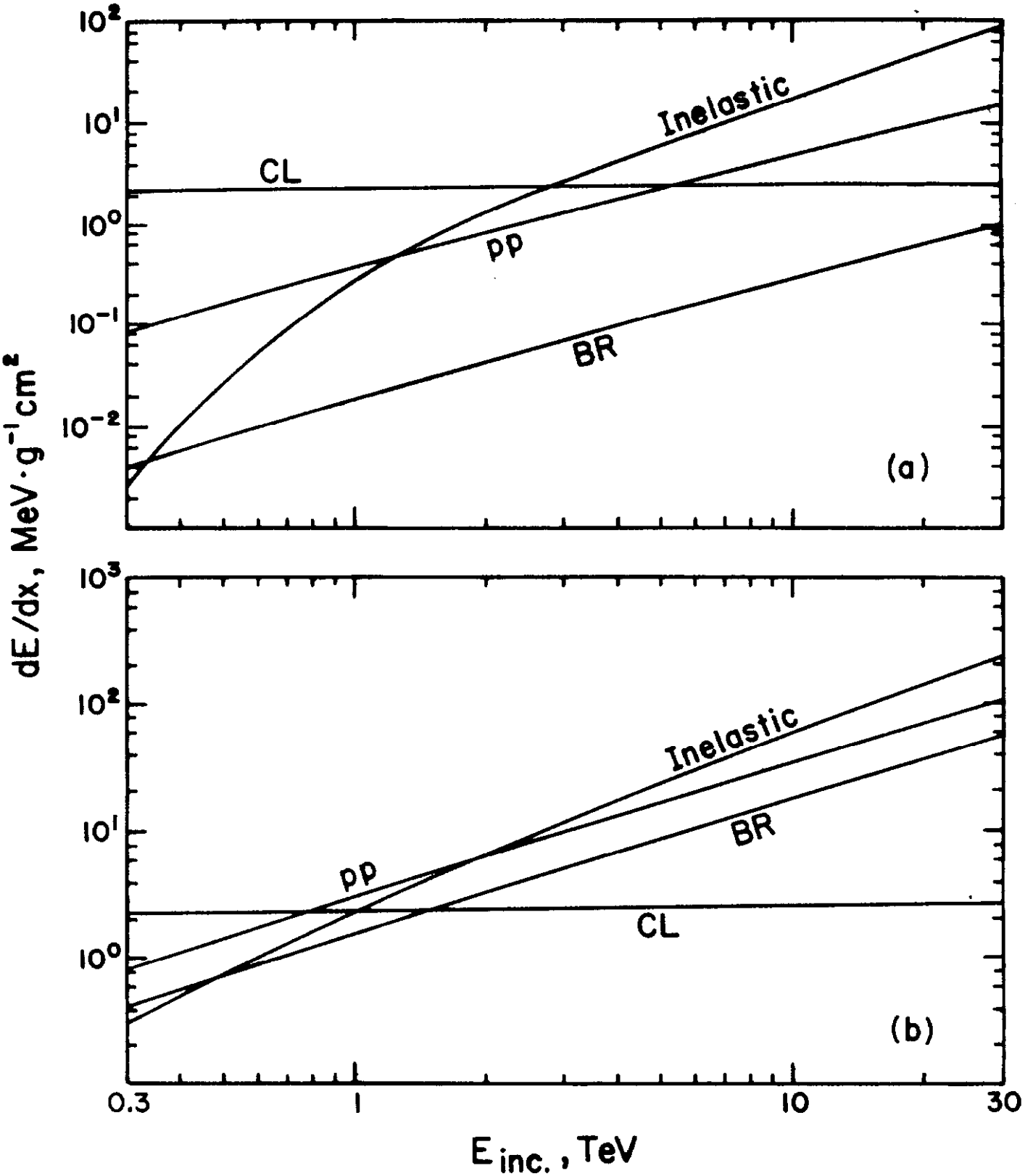
dE/dx, MeV·g⁻¹cm²
Inelastic
CL
pp
BR
(a)
Inelastic
BR
pp
CL
(b)
0.3
1
10
30
E inc., TeV

Fig. 12

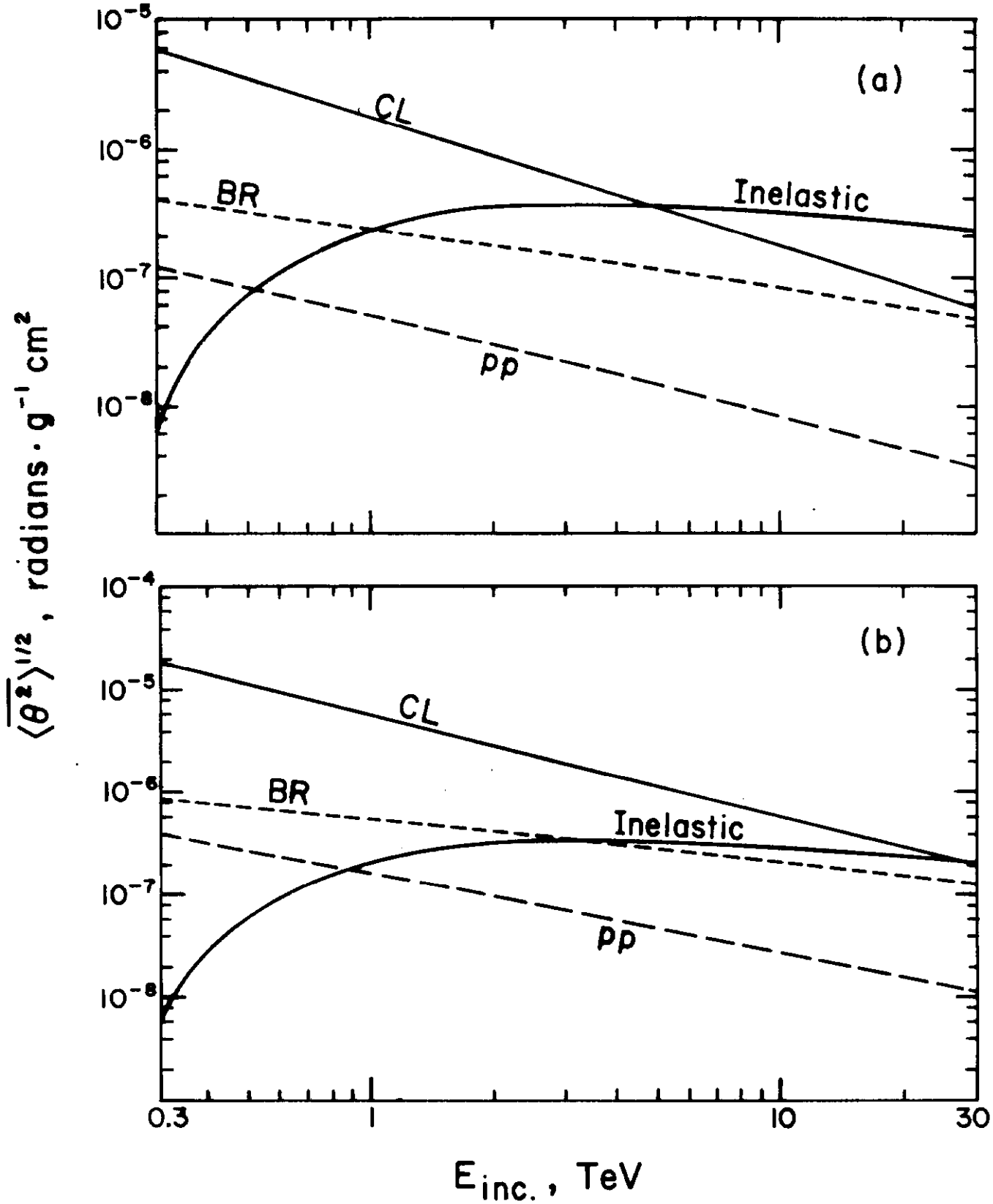
(a)
CL
BR
Inelastic
pp
(b)
CL
BR
Inelastic
pp
$\overline{\langle\theta^2\rangle}^{1/2}$, radians · g^{-1} cm^2
$E_{inc.}$, TeV
0.3
1
10
30

Fig. 13

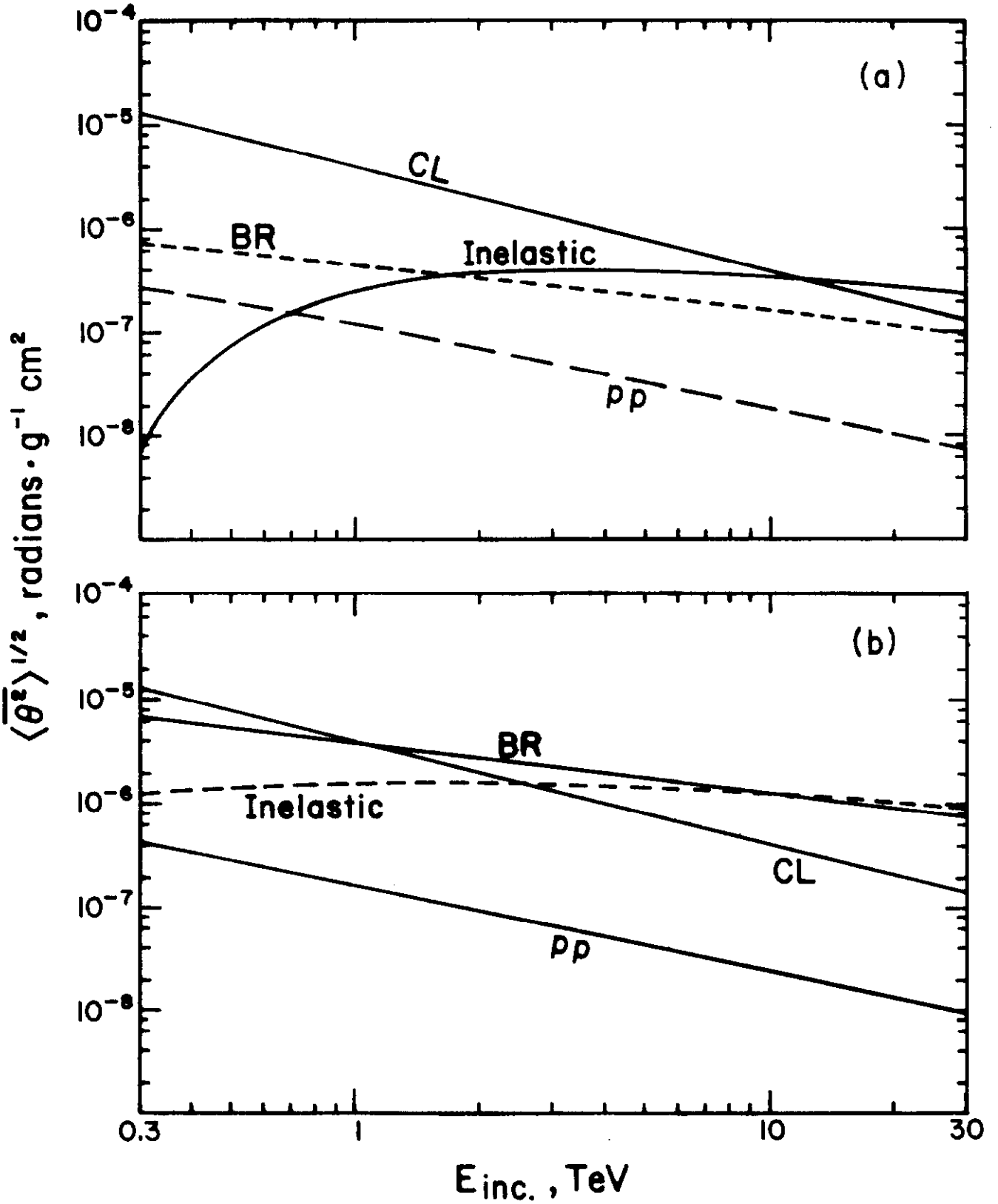
(a)
CL
BR
Inelastic
pp
(b)
BR
Inelastic
CL
pp
$\langle\overline{\theta^2}\rangle^{1/2}$, radians · g^{-1} cm^2
10^{-4}
10^{-5}
10^{-6}
10^{-7}
10^{-8}
0.3
1
10
30
$E_{inc.}$, TeV

Fig. 14